Measurement of the Surface Energy of Unsupported Nanocrystals

Xiaofei Ma, Anshuman Lall, George Mulholland and Michael R. Zachariah
UMD/NIST Co-Laboratory for NanoParticle Based Manufacturing and Metrology
Department of Mechanical Engineering, University of Maryland-College Park

Abstract

A novel method to study the evaporation kinetics of nanocrystals (NC) is developed. Direct *in situ* measurement of mass change using a tandem ion-mobility size and mass spectrometers is used to determine the size dependent evaporation rate. A kinetic model is used to relate the evaporation rate to the temperature dependent surface energy. We report measurements for Zn NC surface energies of 9.0 and 13.6 J/m^2 at 375 ^{0}C and 350 ^{0}C, respectively. We also observed using electron microscopy the crystal edge effects which lead to an evaporation anisotropy for Zn NCs.

Nanoparticles, due to their large surface-to-volume ratio, and finite number of atoms, have demonstrated many physical and chemical properties which significantly differ from the respective bulk material. For example, particle size dependent physical processes such as melting point depression [1-3] (one of the oldest areas of small particle research), size dependent structural transformations [4, 5], increased surface energy [6] and band gap have generated considerable interest in both scientific and technological communities. The starting point for understanding the novel properties of NCs is to study their atomic structure, and one of the fundamental physical quantities in determining the mesoscopic structure is surface energy.

The surface energy is defined as the energy required to create a unit area of new surface. It plays an essential role in nanoparticle processes such as melting, coalescence and evaporation. It also determines the equilibrium shape, faceting and crystal growth of NCs. During the last decade, many theoretical studies on surface energy of metals and semiconductors employing either first-principles or semi-empirical methods have been published [7, 8]. While there exists a fairly broad literature for bulk material, there are only a few experimental studies that report surface energy of NCs. Even for bulk material, most experimental data stems from the liquid phase surface tension measurements, which are extrapolated to the solid [7]. Direct experimental measurement of surface energy for NC's has proven to be difficult due to the obvious size issues and because of the interference between the NC's with its supporting environment. In a recent studies, however, Nanda et al. [6, 9] reported on measurements of surface energies of free (unsupported) Ag, Au, and PbS nanoparticles based on a size dependent evaporation study. Nanda et al. found that using the Kelvin equation [10], the surface energy was fund to be significantly higher than their bulk counterparts. In the interpretation of their results they assumed that the surface energy is not dependent on the particle size and temperature. However, theoretical considerations show that the surface energy is both temperature and particle size dependent [11].

In this study we employ both the size selection and subsequent monitoring of the mass changes using tandem gas-phase ion-mobility methods. Because of the polyhedron shape of NCs and the fact that particle size can change due to density change in the processes such as melting and re-crystalization, direct mass measurement promises to be

a more accurate analysis than monitoring particle size change during evaporation. The experimental measurements are conducted for Zn nanocrystals, but the method is generic. In this way we are able to characterize surface energy without the need for collecting particles and imaging them with a TEM.

The experiment system consists of three components. Preparation of monodisperse Zn particles, exposure of size selected Zn particles into a controlled temperature region, and finally, measurement of the mass change resulting from evaporation. Our experiment consists of two different ion-mobility schemes in series. The first mobility characterization is to size select particles with a differential mobility analyzer (DMA) [12]. The second mobility characterization employs an aerosol particle mass analyzer (APM) [13] and measures changes in mass resulting from a controlled evaporation of the NCs.

Since we are employing ion-mobility methods, particles are first charged with a Boltzmann charge distribution by exposing the nanoparticle aerosol to a Po-210 source, before the DMA. The average charge state of sample particles under Boltzmann distribution is roughly neutral, with most of particles uncharged and equal amount of particles carry +/- 1 charge and +/-2 charges, etc. For example, in case of 50 nm particles, 60.2% particles will be neutral, 19.3% carry +/-1 charge, 0.6% carry +/- 2 charges, and higher charge state would be even less. Considering the small percentage in the multiple charged states, we ignore multiple charged particles. Both the DMA and APM are configured to classify positively charge particles for these experiments.

The DMA, used in this experiment for size selection, consists of an annular region between two concentric cylinders, with the center cylinder held at high voltage and the outer one at ground [12]. Charged particles of the right polarity feel an attractive force toward the center electrode and move radically inward at an electrophoretic velocity determined by the particle charge, and drag force which is a function of particle size. When charged particles flow between the cylinders the electric force on the particle is balanced by the drag force, and at a fixed voltage all particle exiting the instrument have (to the resolution of the instrument) equivalent mobility sizes.. In the size range of consideration here, the DMA functions as a source of mono-area particles [14].

The APM can determine the particle mass distribution based on particle mass to charge ratio, and is used in our experiment to monitor changes to the particle mass resulting from evaporation. The APM consists of two concentric cylindrical electrodes that rotate together at a controlled speed. An electrical field is created by applying high voltage on the inner electrode while the outer one is held at ground. Charged particles flowing within the concentric cylinders experience opposing centrifugal and electrostatic forces and as a result particles exiting the instrument at fixed voltage and rotation speed all have the same nominal mass. By scanning either the voltage or the rotation speed, the particle mass distribution (independent of particle shape) can be determined. APM mass measurements are independent of particle morphology because the centrifugal force is directly proportional to the mass. Our previous experiments have used the DMA-APM technique to measure the inherent density of nanoparticles, as well as to study the mechanism of aluminum and nickel oxidation [15].

Based on operating conditions for the DMA and APM, we estimate uncertainties as follows. For the DMA operating conditions the uncertainty is based on the theoretical transfer function which will give an uncertainly in the peak particle size of +/- 4 %. We then use Gaussian fit to determine the peak size which would have a precision uncertainty of no more than 1%. A similar result can be obtained for the APM however the uncertainties are not due to the transfer function but uncertainties in the step voltage which has a resolution of only +/-0.5V, which gives an uncertainty in mass of ~4%. Using the root-sum-square (RSS) method, we can estimate the uncertainty of density calculation ~5%. This is consistent with prior work (unpublished) using combined DMA/APM on reference aerosols (NaCl and DOP) which gave an experimentally determined uncertainly in density of 4%.

In our study Zn NCs are generated using an evaporation/condensation method in argon. Zn vapor is generated from granular Zn (purity, ≥99.99% from Sigma-Aldrich) by evaporation in a tube furnace at $550^{0}C$ with a flow of argon. Unagglomerated single crystal Zn NCs are formed at the exit of the flow tube by empirical adjustment of the furnace temperature and the argon carrier gas flow rate. In our experiment, Zn NCs of ion-mobility sizes of 50nm, 70nm, 100nm and 150nm were selected in sequential experiments to study the size-dependent evaporation.

After size classification, a second tube furnace enables the controlled evaporation of the NCs. The residence time of the aerosol in this furnace is about 5 seconds at a flow rate of carrier gas of 0.5 SLPM. To monitor the small mass change of the NCs due to evaporation, an aerosol particle mass analyzer is placed downstream. Particles exiting the APM will be selected on the basis of mass and are counted using standard particle counting methods using a condensation particle counter.

In the experiment, the temperature in the evaporation furnace was set between 250 - $400^{\circ}C$ in increments of $25^{\circ}C$. The particle mass distribution was then measured for each furnace temperature after the system reached steady state. The room temperature particle mass distribution was also taken, and set as the base of the mass measurement. Samples for electron-microscopic analysis were collected exiting the evaporation furnace by electrostatically precipitating the aerosol onto a TEM grid.

Zn has a hexagonal close-packed crystal structure. Figure 1(a) shows SEM images of two single Zn NCs which clearly exhibit the shape of perfect hexagonal prism. EDS spectra obtained from the NCs in SEM confirmed that the composition as Zn. Selected area electron diffraction analysis indicated that the Zn NCs have top surfaces of {0001} crystal planes and side surfaces of $\{1\bar{1}00\}$ planes.

A typical plot of normalized mass distributions of Zn NCs classified by the DMA operated at a fixed mobility size at different evaporation temperature is shown in the Figure 2(a). To study the size-dependent evaporation behavior of Zn NCs, the peak mass in Figure 2(a) is plotted against the temperature. The plots is shown in Figure 2(b) and can be categorized as falling into two regions, which can be represented by the best linear fits to the data. The near horizontal line represents the un-evaporated case, in which the mass of the NCs doesn't change, while the steeply sloped straight line represents an evaporation case. The onset temperature for evaporation for each mobility size is determined by finding the intersection of the temperature lines. Even for the largest size of NCs $(150nm)$, the onset temperature of evaporation is lower than the bulk melting temperature of Zn $(692K)$, and the boiling temperature $(1180K)$. This result is also consistent with the experimental observation of PbS and Ag nanoparticles [6, 9].

Before we turn to interpreting the experimental ion-mobility results we note the strong anisotropy during NC evaporation and morphology evolution. This can be seen from the SEM images of partially evaporated Zn NCs in Figure 1(b). Most of the hexagonal-shaped top surfaces (Zn {0001} planes) of the Zn NCs during evaporation are well-preserved relative to the side surfaces (Zn $\{1\bar{1}00\}$ planes). Material from the side surfaces are preferentially etched away, which leaves the side surfaces with a depression while the top surfaces remain perfectly planar. The reader is reminded that the evaporation takes place in the gas phase prior to deposition of the NC on the TEM grid. A reasonable explanation for this phenomenon is that atoms on the edges are unstable compared with the atoms on a flat surface. Once the evaporation starts, edge atoms always leave the crystal first. The evaporation of edge atoms thus promotes the unzipping of adjacent atoms from the crystal planes. Since the side surfaces have more edges than the top surfaces, the evaporation from the side surfaces is enhanced.

To interpret the results and extract surface energy, we evaluate the evaporation rate from gas kinetic theory. The particle mass change rate due to evaporation from a small particle (Kn > 1) is given by [16]: $\frac{dm}{dt} = \frac{\rho \alpha S v_m (p_1 - p_d)}{(2\pi m_m k_B T)^{1/2}} \cdots\cdots (1)$,

Where m is the mass of the NC, α is the accommodation coefficient, S is the surface area of the NC, v_m is the atomic volume of the condensing species, p_1 is the vapor pressure of the condensing species in the environment, p_d is the vapor pressure of the condensing species at the particle surface, m_m is the atomic mass of the condensing species and the k_B is the Boltzmann constant. If we assume the surface area of the NCs doesn't change during the initial stage of the evaporation (a valid assumption since the mass change of the NCs in the furnace is very small compared with the initial mass of the NCs, i.e. the surface area change of NC can be neglected.) we can convert equation (1) from a differential to an algebraic equation: $\Delta m = \frac{\rho \alpha S v_m (p_1 - p_d)}{(2\pi m_m k_B T)^{1/2}} \Delta t \cdots\cdots (2)$,

Where Δm is the mass change of the NCs over a residence time Δt of ~5 seconds. For crystalline particles, the vapor pressure at the NC surface can be calculated using the Kelvin equation for small crystals [17] $p_d = p_s \exp(\frac{2\gamma_i M}{\rho R T r_i}) \cdots\cdots (3)$

Where γ_i is the surface energy, M is the molecular weight, ρ is the density of NC, R is the gas constant, T is the temperature and r_i is the vector length proportional to the magnitude of surface energy of each NC face from a common origin.

Since in the experiment, materials only seems to evaporate from the $\{1\bar{1}00\}$ planes only**,** so r_i in equation (3) is actually the vector length r normal to the $\{1\bar{1}00\}$ plane of the Zn NC measured from the center of the hexagonal prism. Based on the room temperature particle mass measurement and the c/a ratio of the synthesized NCs, we obtain the r_i corresponding to the side surfaces to be 19.8, 27.7, 40.0 and 56.8 nm corresponding to NCs of initial mobility diameters 50, 70, 100 and 150 nm, respectively. In equation (3), p_s is vapor pressure over a flat surface, we use the expression $\log p_s(\text{pascal}) = 5.006 + 6.102 - \frac{6776}{T(K)}$.....(4) [18] to find p_s at a given temperature. Compared with p_d, the environmental vapor pressure p_1 is essentially zero for the reason that the DMA dilutes the aerosol flow before the NCs enter the evaporation furnace and the contribution of Zn vapor pressure due to the evaporated Zn materials in the furnace is much smaller than the saturation vapor pressure at that temperature. Since when evaporation begins, materials only evaporate from the $\{1\bar{1}00\}$ plane (side surfaces). The surface area S in equation (2) can be approximated by $6ac$ (the total area of side surfaces). The surface energy thus calculated is for the $\{1\bar{1}00\}$ planes of Zn NC. If we plug in v_m, m_m and M for Zn, the only two free parameters remaining in the equation (2) are α the accommodation coefficient and γ the surface energy. Both α and γ are believed to be temperature dependent, and independent of particle size at the size range in our experiment. The calculation yields a surface energy $\gamma = 13.6 J/m^2$ at $350^\circ C$, and

$\gamma = 9.0 J/m^2$ at $375^\circ C$ for Zn $\{1\bar{1}00\}$ planes. The polyhedron shape of Zn NCs shows the strong surface energy anisotropy.

To further verify our results, we modified the method described in reference [6, 9] to calculate the surface energy. The onset temperature of evaporation is plotted against the inverse of $2r_{\{1\bar{1}00\}}$ as shown in Figure 3. From the plot, we can see that the onset temperature of evaporation decreases with the decrease of particle size. This is consistent with the observations of Nanda et al. It is possible that both Kelvin equation and the edge effect contribute to the strong size dependent evaporation of NCs. As the NC size decreases, the vapor pressure over the NC surface tends to be higher due to Kelvin effect which favors the evaporation. Also, as the NC size shrinks, there is a larger fraction of total atoms at the crystal edges which are unstable upon heating. A linear relationship between the onset temperature of evaporation and the inverse of the NC size is found by fitting the experimental data. The best fit line yields a slope of $-2308.6 nm \cdot K$ and an intercept of $657.85 K$, the latter representing the temperature where very large particles start to evaporate. Using equations (3) and (4) we calculate the surface energy γ to be $10.1 J/m^2$. Since this method doesn't consider the temperature effect on the value of surface energy, the surface energy calculated this way can be regarded as the temperature average of the surface energy for Zn NCs. The value $10.1 J/m^2$ is in reasonable agreement with the values calculated using the kinetic equations. In contrast, a surface energy of 0.993 J/m^2 has been obtained for bulk zinc by Tyson in his experiment work [19]. Vitos and his coworkers [7] applied a full charge density (FCD) linear muffin-tin orbitals (LMTO) method, and calculated the surface energy of bulk Zn (0001) plane to be 0.989 J/m^2. However, this high surface energy may be partially due to the difference in physical processes between our experiment approach (based on NC evaporation) and others' (based on natural dividing surfaces) [20]. The main difference between the two cases lies in the coordination numbers of an surface atom [21], and this leads to the difference in cohesive energy per atom. In brief, the cohesive energy per atom in the evaporation method must be multiplied by z/2 (z is the coordination number of the crystal material) to compare with that of the natural dividing case. Thus, the surface energy of Zinc NC calculated using evaporation method should be at least 6 times (since the

coordination number of hcp crystal is 12) larger than the bulk value. Apart from the difference between the physical processes, the high surface energy of Zn NC can be attributed as an intrinsic property of free NCs.

In summary, we have successfully generated size-classified Zn NCs and have demonstrated that the size-dependent evaporation of free Zn NCs can be studied by an in-flight tandem DMA-APM method. The variation of the onset temperature of evaporation with the size of NCs is found to be similar to the melting temperature depression of small nanoparticles. This gives direct evidence of the Kelvin effect. We also observed the edge effect in the evaporation process of NCs using electron microscopy. The surface energy of Zn NCs has been estimated by using a simple kinetic model, the surface energy of Zn $\{1\bar{1}00\}$ planes is found to be 13.6 J/m^2 at 350C and 9.0 J/m^2 at 375C. These values are consistent with the value of 10.1 J/m^2, which is calculated by plotting the onset temperature of evaporation vs. inverse $2r_{\{1\bar{1}00\}}$

This work is partially supported by the Army Research Office, the University of Maryland Energy Research Center (UMERC). Partial support for electron microscopy was provided by the University of Maryland MERSEC.

Refrences

1. Goldstein, A.N., C.M. Echer, and A.P. Alivisatos, *Melting in Semiconductor Nanocrystals.* Science, 1992. **256**(5062): p. 1425-1427.
2. Lai, S.L., et al., *Size-dependent melting properties of small tin particles: Nanocalorimetric measurements.* Physical Review Letters, 1996. **77**(1): p. 99-102.
3. Schmidt, M., et al., *Irregular variations in the melting point of size-selected atomic clusters.* Nature, 1998. **393**(6682): p. 238-240.
4. Ajayan, P.M. and L.D. Marks, *Experimental-Evidence for Quasimelting in Small Particles.* Physical Review Letters, 1989. **63**(3): p. 279-282.
5. Cleveland, C.L., et al., *Structural evolution of smaller gold nanocrystals: The truncated decahedral motif.* Physical Review Letters, 1997. **79**(10): p. 1873-1876.
6. Nanda, K.K., et al., *Higher surface energy of free nanoparticles.* Physical Review Letters, 2003. **91**(10).
7. Vitos, L., et al., *The surface energy of metals.* Surface Science, 1998. **411**(1-2): p. 186-202.
8. Zhang, S.B. and S.H. Wei, *Surface energy and the common dangling bond rule for semiconductors.* Physical Review Letters, 2004. **92**(8).
9. Nanda, K.K., F.E. Kruis, and H. Fissan, *Evaporation of free PbS nanoparticles: Evidence of the Kelvin effect.* Physical Review Letters, 2002. **89**(25).
10. (Kelvin), W.T., Philos. Mag., 1871. **42**: p. 448.
11. Medasani, B., Y.H. Park, and I. Vasiliev, *Theoretical study of the surface energy, stress, and lattice contraction of silver nanoparticles.* Physical Review B, 2007. **75**(23).
12. S.H. Kim, B. Y.H. Liu and M.R. Zachariah *"Method for Measuring the Charge and Size Distribution of NanoAerosols"* Journal of Colloid and Interface Science **282**(1), 46-57 (2005)
13. Ehara, K., C. Hagwood, and K.J. Coakley, *Novel method to classify aerosol particles according to their mass-to-charge ratio - Aerosol particle mass analyser.* Journal of Aerosol Science, 1996. **27**(2): p. 217-234.
14. SCHMIDT-OTT, A., *NEW APPROACHES TO IN SITU CHARACTERIZATION OF ULTRAFINE AGGLOMERATES.* J. Aerosol Sci, 1988. **19**(5): p. 553-563.
15. Lei Zhou, A.R., Nicholas Piekiel, Xiaofei Ma, Michael R. Zachariah, *Ion-Mobility Spectrometry of Nickel Nanoparticle Oxidation Kinetics:*

Application to Energetic Materials. The Journal of Physical Chemistry c in press, 2008.

16. Friedlander, S.K., *SMOKE, DUST, AND HAZE Fundamentals of Aerosol Dynamics*. Second ed. 2000.
17. W.J.Dunning, *General and Theoretical Introduction*. Nucleation, ed. A.C.Zettlemoyer. 1969, New York: Marcel Dekker, Inc.
18. *Handbook of Chemistry & Physics* CRC Press.
19. Tyson, W.R. and W.A. Miller, *Surface Free-Energies of Solid Metals - Estimation from Liquid Surface-Tension Measurements.* Surface Science, 1977. **62**(1): p. 267-276.

20. Ouyang, G., X. Tan, and G.W. Yang, *Thermodynamic model of the surface energy of nanocrystals.* Physical Review B, 2006. **74**(19).
21. Vanithakumari, S.C. and K.K. Nanda, *Phenomenological predictions of cohesive energy and structural transition of nanoparticles.* Journal of Physical Chemistry B, 2006. **110**(2): p. 1033-1037.

Figures

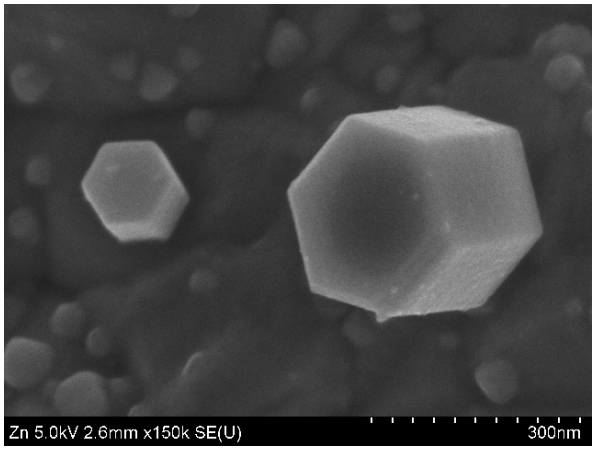

(a)

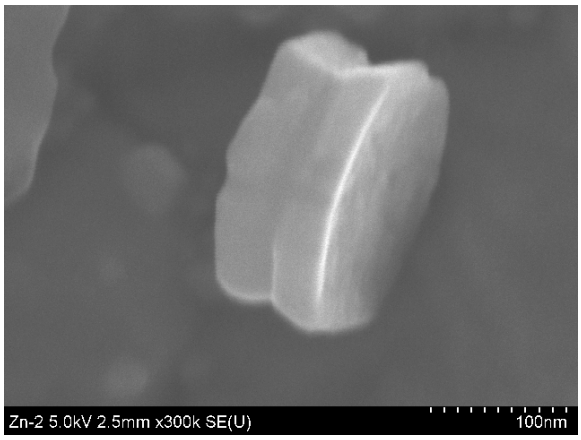

(b)

Figure 1 SEM images of as aerosol grown hexagonal-prism-shaped Zn nanocrystals (a) before evaporation (b) partially evaporated Zn NC

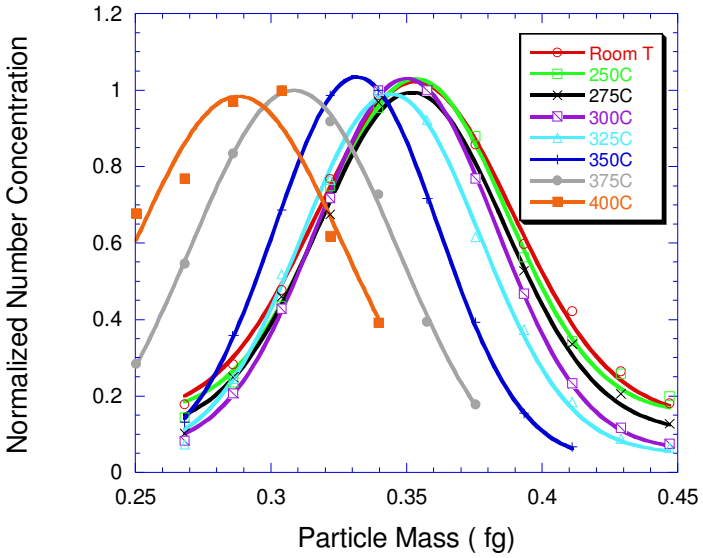

(a).

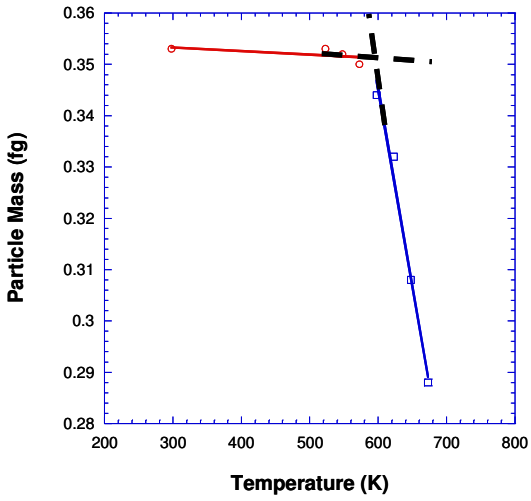

(b)

Figure 2 (a) Normalized particle mass distributions for initial mobility particle size of 50nm NCs at different evaporation temperatures. (b) Particle mass vs. temperature for initial particle size of 50nm NCs

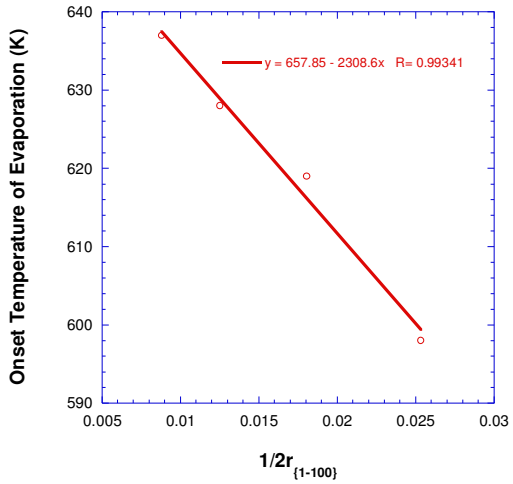

Figure 3 Onset temperature of evaporation vs. $1/2r_{\{1\bar{1}00\}}$